Predicting low-velocity impact damage in composites by a quasi-static load model with cohesive interface elements

X. Zhang
xiang.zhang@cranfield.ac.uk
F. Bianchi
Aerospace Engineering Dept
Cranfield University
Bedford, UK

H. Liu
AVIC First Aircraft Institute
Xi'an, China

ABSTRACT

A numerical model is developed for predicting low-velocity impact damage in laminated composites. Stacked shell elements are employed to model laminate plies with discrete interface elements in pre-determined zones to model the onset and propagation of matrix cracks and delamination. These interface elements are governed by a bi-linear cohesive failure law. Cohesive element zone size is determined by a separate finite element analysis using solid elements to identify the stress concentration sites. In order to save the computational effort, low-velocity impact load is modelled by quasi-static loading. Influence of contact force induced friction on shear driven mode II delamination is modelled by a friction model. For a clustered cross-ply laminate, calculated impact force and damage area are in good agreement with the test results. It is shown that matrix cracks should be included in the model in order to simulate delamination in adjacent interface. The practical outcome of this research is a validated modelling approach that can be further improved for predicting low-velocity impact damage in other stacking sequences.

Paper No. 3855. Manuscript received 19 June 2012, accepted 30 October 2012.

https://doi.org/10.1017/S0001924000007685 Published online by Cambridge University Press

NOMENCLATURE

E	laminate equivalent membrane elastic modulus
G_{IC}, G_{IIC}, G_{IIIC}	interlaminar fracture toughness in mode I, II, III, respectively
K_1, K_2	stiffness of cohesive element and contact node pair, respectively
K_N, K_S, K_T	stiffness of cohesive law in mode I, II, III, respectively
N	critical stress of cohesive law (mode I)
P	applied contact (indentation) force
P_c, P_f	contact force, friction force
P_{cr}	critical impact force
S	critical stress of cohesive law (mode II)
t	laminate thickness
T	critical stress of cohesive law (mode III)
δ	indentation displacement
ν	laminate equivalent Poisson's ratio
μ	coefficient of friction for the contact node pairs in the numerical model
μ_a	actual coefficient of friction
CZM	cohesive zone model
QSL	quasi-static load

1.0 INTRODUCTION

Current damage-tolerance design criteria for compression-loaded composite airframe structures are related to the impact energy or the depth of the dent in the structure caused by the impact event. The problem, issues and approaches to low-velocity impacts representing dropped tools and runway debris are well described in[1-3]. Testing of all candidate materials and configurations at various structural levels is virtually impossible. On the other hand, the structural behaviour under impact is very complex with matrix cracks and delaminations forming at different locations and interacting with each other. Therefore, many researchers have focused their attention on numerical modelling and simulation aiming at developing computer-based design tools. For example, strength-based failure models have been employed for predicting damage initiation[4-7]. The well-known Chang-Chang model was originally developed for predicting in-plane fibre and matrix damage[4-5]. Although laminated composite plates can be treated as layered two-dimensional anisotropic plates since there are no significant through-thickness stresses except at the free edges, this is manifestly not true for normal point impacts. To predict impact damage, Chang-Chang's model was improved by including interlaminar shear and peel stresses[6-7]. Recently, Bouvet *et al*. employed a much detailed FE model using spring elements to calculate interlaminar stresses at damage zones and then use strength based failure criterion to model damage propagation (both in-plane and out-of-plane)[8]. Although the FEM is fairly accurate for predicting the impact force response, it is still crude for stress calculations. Moreover, calculated stresses are also dependent on the mesh size. Therefore, the majority of researchers have turned to the fracture mechanics based methods, especially for predicting delamination propagation[9-10]. Most commercial computer packages can perform calculations of the crack front strain energy release rates. This method works well if pre-cracked structural models are realistic and using suitably shaped mesh. For irregular shaped delamination the adaptive mesh approach is recommended. Recently, cohesive zone models have been used to model both initiation and propagation under impact loads[11-12]. Detailed reviews of these methods can be found in Refs 13-14.

https://doi.org/10.1017/S0001924000007685 Published online by Cambridge University Press

This paper presents a finite element model of laminated composite plates subjected to quasi-static loading (QSL) aiming at developing a more efficient numerical model for predicting low-velocity impact force and impact damage including in-plane matrix fracture and interlaminar delamination.

2.0 MODELLING APPROACH

2.1 QSL *vs* low-velocity impact test

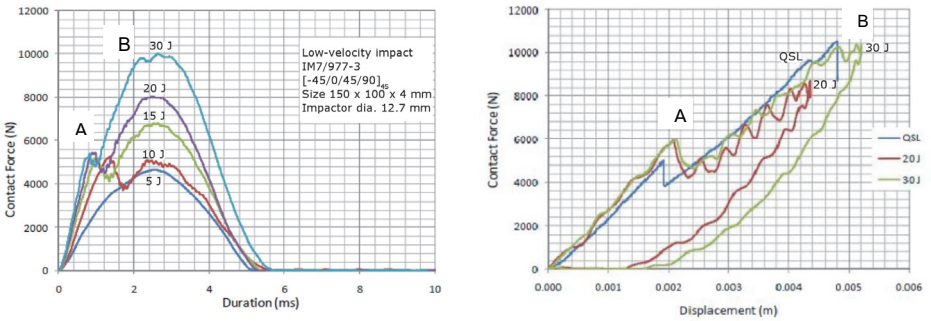
It has been well established that a critical impact force (P_{cr}) exists that corresponds to delamination onset and is proportional to $t^{3/2}$ [15-18]. As an example, filtered impact force *vs* time histories for five individual impact tests at increased incident energy on 4mm thick quasi-isotropic laminates are shown in Fig. 1(a)[19]. A critical impact force of about 5·4kN can be clearly observed which is the first load-drop point. This measured critical force is very close to a predicted value of 4·8kN using Equation (1)[16-17]:

$$P_{cr} = \sqrt{\frac{8\pi^2 E t^3 G_{IIC}}{9(1-\nu^2)}} \quad \ldots (1)$$

Pre-preg used in Brindle and Zhang(2009) was IM7/977-3. According to material manufacturer's data[20], $G_{IIC} = 580\text{J/m}^2$, and calculated laminate equivalent elastic properties $E = 61\text{GPa}$, $\nu = 0{\cdot}31$.

Critical impact force is a useful parameter for correlating the specimen size effect including impact on the skin of realistic skin-stringer panels as long as the laminate layup and thickness are the same[17,21]. It can aid the design process by relating coupon test data with realistic structural panels as long as the thickness and stacking sequences are the same. However, modelling impact dynamic response in composites is computationally demanding especially when including various damage modes and damage propagation.

To develop a computationally efficient model (for design tools), QSL indentation tests were firstly performed to make comparisons with low-velocity impact test[19]. Static indentation load is applied at the plate centre by displacement-controlled loading. Reaction force *vs* deflection curves of two impact tests (at incident energy of 20J and 30J) and a QSL test are shown in Fig. 1(b). Hysteresis plots were recorded in the low-velocity impact tests whereas the QSL test was terminated at the maximum failure load. The two types of test agree well within a narrow margin. The first load-drop



(a) (b)

Figure 1. Experimental test results of low-velocity impact and quasi-static loading[19].
(a) Impact force *vs* time history (filtered), (b) Force *vs* displacement; QSL and impact tests (unfiltered)

https://doi.org/10.1017/S0001924000007685 Published online by Cambridge University Press

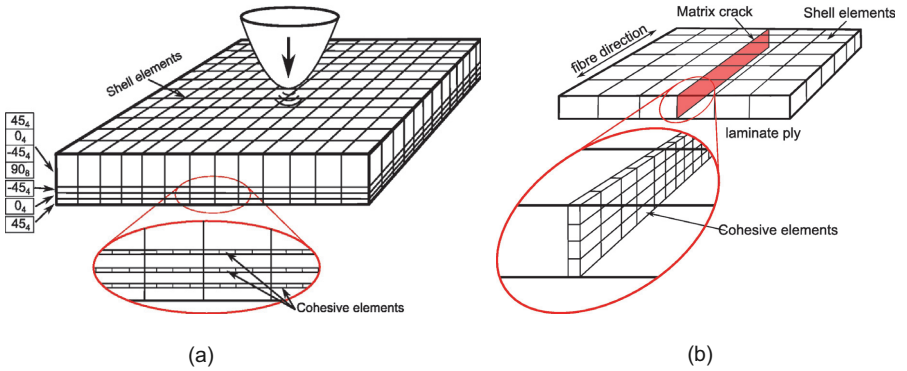


Figure 2. Cohesive interface elements for modelling:
(a) multiple delaminations; (b) in-plane matrix cracking in back-face ply.

point (A) at 5kN and the peak load point (B) are recognised in both types of tests. Peak forces at these load-drop points are also comparable indicating the equivalence between low-velocity impact and quasi-static load tests subjected to equivalent impact-point deflection. It is worth mentioning that the higher critical impact force of 6kN for the two impact tests was measured from unfiltered test data that could include certain level of high frequency noise. The filtered data shown in Fig. 1(a) shows a critical force of about 5·4kN, which is the same as that of the QSL test. With this equivalence and assuming the influence of inertia is negligible at low velocity, QSL numerical models can save considerable amount of computation time. This point is confirmed by the research conducted by Sjoblom *et al*[22], which shows that the relation between impact force and displacement is not changed by the impact velocity in the low-velocity ranges. Damage size and failure modes are also comparable between the quasi static and dynamic (low-velocity impact) tests.

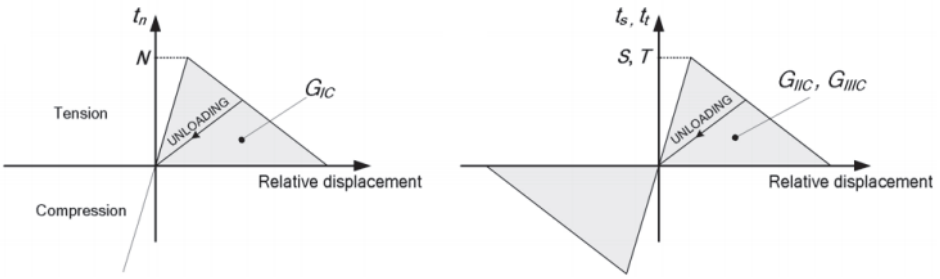
2.2 FE model

A rectangular test coupon is modelled using the commercial software package ABAQUS[23]. The laminate is modelled by continuum shell elements with assembled mechanical properties. To model interlaminar damage initiation and propagation, shell elements are stacked with each element layer representing either one lamina ply or several plies. Cohesive interface elements are placed between the shell element layers as shown in Fig. 2(a). To model the in-plane matrix cracking, cohesive elements are also placed within the lamina plane (Fig. 2(b)) along the line where the in-plane stress transverse to fibre direction(σ_{22}) is expected to be high enough to cause matrix cracking. This is the ply on the back face of the coupon, where impact-induced bending stress is in tension and at the highest value.

2.3 Cohesive law for interface elements

Several cohesive failure models exist governing the surface traction-separation relation of a fracture interface. In this study, a bilinear traction-separation law is used as shown in Fig. 3. Some studies suggest that model prediction is not sensitive to the cohesive law used as long as the fracture toughness value (G_C) is the same[24-25]. This is true only in the case where pure damage models are used and the strain rate effects are negligible. Value of G_C is the integration area of the traction stress *v*s separation displacement curve shown in Fig. 3.

https://doi.org/10.1017/S0001924000007685 Published online by Cambridge University Press



(a) (b)

Figure 3. Traction-separation laws for: (a) mode I, and (b) model II and III delamination (adopted from[11]).

2.4 Influence of friction on delamination

Due to the Hertzian contact stress, the upper interface of the laminate is subject to high interlaminar shear stresses close to the contact load point. Consequently, peak shear stress can exceed the shear strength of the material (an example of calculated stresses is given in Section 3). However, at the upper interface only very small (negligible) delamination was found in experimental tests as reported in the open literature (e.g. 26). It is believed that the high contact stress on the top interface can inhibit the shear-driven delamination. However, if the mode II cohesive law shown in Fig. 3(b) is used in the FE model, predicted delamination area in the upper interface is of the same order of magnitude as the delamination size at the lower interfaces, which is much larger than measured in tests.

In this paper the influence of contact stress on shear dominant delamination is treated by adding the contribution of contact-induced friction (between adjacent plies) to the constitutive model of the interface element that is governed by a mode II cohesive failure law. Consequently, the friction stress at the delamination crack face will inhibit the delamination propagation rate. This can be achieved by employing either a user-defined cohesive element or a contact algorithm that can increase the contact stiffness during the progressive contact process to prevent the upper ply from penetrating into the lower ply. In this paper, a simple contact relationship is set up between the two layers of shell elements where there is a layer of interface cohesive elements, aiming at introducing friction stress between the two plies where delamination will initiate and propagate. As illustrated in Fig. 4, this contact model acts in parallel with the interface elements that have zero thickness in order to satisfy the contact condition. Therefore, the total applied force is transferred into the laminate by two mechanisms: the contact model

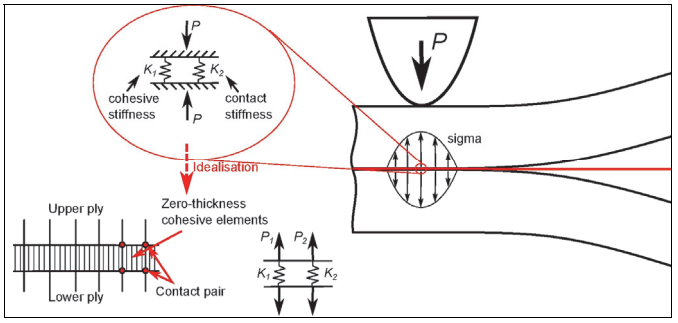


Figure 4. Schematic of cohesive elements, contact node pairs and implementation into FE model.

https://doi.org/10.1017/S0001924000007685 Published online by Cambridge University Press

and the cohesive model, which act as two springs in parallel. The cohesive element is used for modelling damage propagation, whereas the contact node pair is able to transfer the friction stress. The cohesive elements and contact node pairs are connected to the surrounding shell elements by shared nodes, i.e. the cohesive elements are connected to the shells elements by forcing the cohesive element nodes to stay on the shell element surface, and the shell element nodes are also used for the contact node pairs. The forces transferred are then integrated over the element surface and the contributions from the cohesive elements and contact node pairs are summed. This model is implemented into the ABAQUS code without the need of defining any special element.

The fraction of the total applied force carried by the two models is determined by the respective stiffness of the cohesive element and the contact model. The tension stiffness of the cohesive element is determined by the bilinear traction-separation law. However, under the compressive load condition, the original normal stiffness still exists in order to stop penetration between the two adjacent plies. This normal stiffness is retained in the model even after the complete failure of the cohesive elements[11, 26]. In this paper, the cohesive element stiffness does not degrade under compression after the onset of delamination, and the contact node pair is assigned a fixed stiffness equal to the compressive stiffness of the cohesive element. The contact stress is equally distributed between the cohesive elements.

Since the indentation displacement (δ) is the same in the interface elements and the contact nodes, forces transferred by the interface element (P_1) and by the contact node pair (P_2) is calculated as:

$$P_1 = K_1\delta \text{ and } P_2 = K_2\delta \quad \ldots (2)$$

where P_2 is the contact force P_c.
Given that the total applied force (P) equals to $P = P_1 + P_2$, the displacement (δ) can be calculated by:

$$\delta = \frac{P}{K_1 + K_2} \quad \ldots (3)$$

It should be noted that Equation (3) is also valid before the initiation of delamination, because the normal compressive stiffness of the cohesive elements does not degrade.

Finally, the contact force and friction force (P_f) are calculated by:

$$P_c = P_2 = K_2\delta = \frac{K_2}{K_1 + K_2} P \quad \ldots (4)$$

$$P_f = \mu P_c = \mu P \frac{K_2}{K_1 + K_2} \quad \ldots (5)$$

where μ is the coefficient of friction used in the FE contact model to be presented in Section 3.

Since the contact model only transfers a fraction of the total applied contact force, the actual friction coefficient (μ_a), which is used for calculating the friction force from the total applied contact force (P) is:

$$\mu_a = \mu \frac{K_2}{K_1 + K_2} \quad \ldots (6)$$

μ_a should be within the range of experimentally measured friction coefficients among fibre reinforced epoxy composites. A sensitivity study of this parameter is given in Section 3.4.

https://doi.org/10.1017/S0001924000007685 Published online by Cambridge University Press

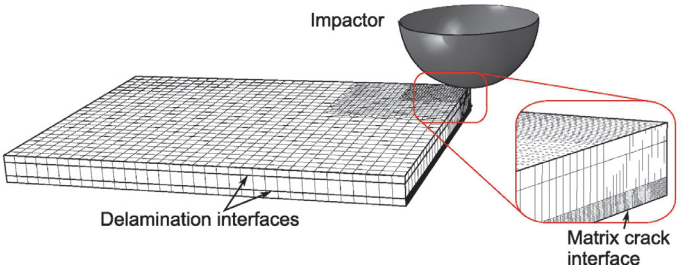


Figure 5. FE model of a quarter of test specimen under quasi-static load (Note the two interfaces in the cross-ply laminate $(90_3/0_6/90_3)$).

3.0 EXAMPLE AND DISCUSSION

A published low velocity impact test[11] was modelled. Test specimen of 87·5 × 65mm in size was fabricated from Seal HS160/REM unidirectional carbon/epoxy prepreg with stacking sequence $(90_3/0_3)_s$ resulting in 2mm nominal thickness. The specimen was simply supported in test by a steel plate with a rectangular cutout of 67·5mm × 45mm underneath the specimen. The diameter of the hemispherical impactor was 12·5mm.

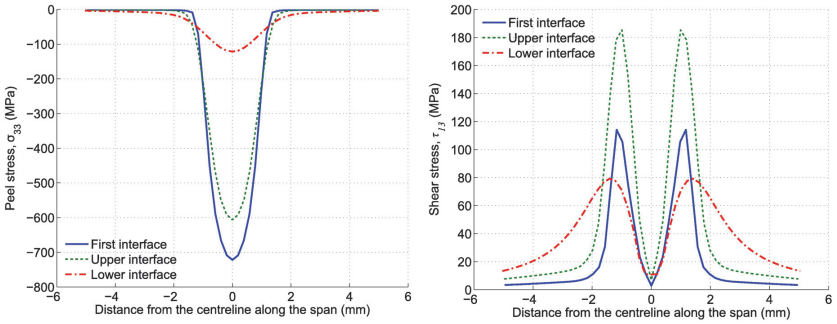
Only one quarter of the specimen was modelled due to the geometric symmetry. The size of the FE model is 67·5mm × 45mm equal to the same size of the rectangular cutout on the supporting frame. The four edges of the specimen are modelled by simply supported boundary condition. Continuum shell elements and cohesive elements are employed to model the laminate and pre-defined interfaces, respectively, as described in Section 2. Since no delamination was expected between the plies of the same fibre orientation, cohesive interface elements were only inserted between the plies having different fibre orientations. For the stacking sequence $(90_3/0_6/90_3)$, two interfaces are modelled by cohesive elements, i.e. the upper interface 90/0 and lower interface 0/90. At the lower interface, where matrix cracking is more critical (due to large bending-induced stresses), an interface of cohesive elements was also inserted to model the matrix cracking (Fig. 5). This cohesive element layer was placed in parallel with the local fibre orientation on the specimen symmetry plane. The smallest shell element size in the impact zone is 0·25 × 0·25mm and the cohesive element size is 0·05mm. It was found necessary to use much smaller cohesive elements, about 1/5 of the surrounding shell element size[27], in order to degrade material properties in damage zones progressively in much smaller area than surrounding element size (to avoid sharp change of material properties and to ensure numerical convergence).

Dynamic transit analysis was performed in Ref. 11 using ABAQUS/Explicit code and solid elements, whereas in this study ABAQUS/Standard code was used for the quasi-static load model. The impactor was modelled as a rigid body indentor. This is reasonable due to the relatively smaller deformation of the impactor compared with the laminate. Laminate elastic properties and cohesive model parameters used in the FE model are given in Table 1, in which symbols

Table 1
Laminate elastic properties and cohesive element parameters used in this analysis (data from Aymerich(2009))

Laminate	Cohesive model (Fig. 3)
E_{11} = 93·7GPa; $E_{22} = E_{33}$ = 7·45GPa (Stiffness)	K_N = 120GPa/mm; $K_S = K_T$ = 43GPa/mm
$G_{12} = G_{23} = G_{13}$ = 3·97GPa	N = 30MPa; $S = T$ = 80MPa (Critical stress)
$\nu_{12} = \nu_{23} = \nu_{12}$ = 0·261	G_{IC} = 520J/m^2; $G_{IIC} = G_{IIIC}$ = 970J/m^2

https://doi.org/10.1017/S0001924000007685 Published online by Cambridge University Press



(a) Peel stress (b) Shear stress

Figure 6. Interlaminar stress distribution along the plate span in three interfaces of a cross-ply laminate ($90_3/0_6/90_3$)).

describing the cohesive model can be found in Fig. 3. In the numerical model, the cohesive element stiffness is 120GPa/mm, which is a typical value for cohesive elements found in the literature. The contact nodes stiffness is also set as 120GPa/mm.

3.1 Stress analysis in undamaged plate

First, FE analysis of residual stresses arising from elevated temperature curing process was performed. Residual transverse shear stresses are found to exist only at the free boundaries of the specimen, which should have little effect on the impact response at the specimen centre. However, in-plane residual stresses transverse to fibre orientation are uniformly distributed across the specimen span with an average value of 35MPa, which is about 50% of the epoxy resin tensile strength. Due to the magnitude of this initial stress, matrix cracking can occur first during impact loading, which subsequently promotes delamination at the adjacent interface. This was also reported in[28].

For undamaged specimens, analysis was performed using solid elements with one element per ply. For an impact energy of 1·5J, the maximum deflection at the specimen centre was measured as 1·88mm. This displacement is applied in the QSL model resulting in a reaction contact force of 1,640N. Fig. 6 shows the stress distributions at three interfaces, i.e. the first interface between the top face plies (90/90), the 'upper interface' (90/0) and 'lower interface' (0/90). For the (90/0)

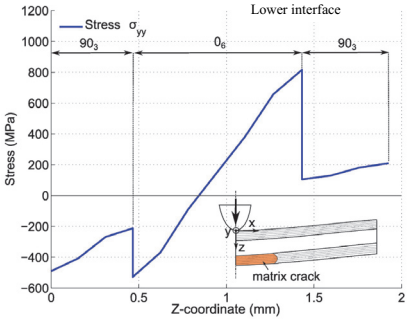


Figure 7. In-plane transverse stress ($\sigma_{22} = \sigma_y$) distribution through the thickness of cross-ply ($90_3/0_6/90_3$). Note: σ_{22} at the lower interface (0/90) is about 100MPa.

https://doi.org/10.1017/S0001924000007685 Published online by Cambridge University Press

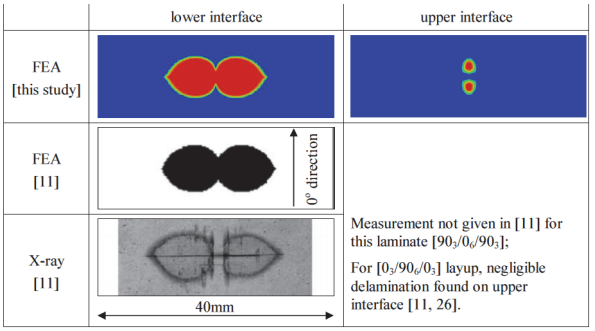


Figure 8. Predicted delamination size and experimental measurement (impact energy 1·5J; μ = 0·9 is used in the FE model).

and (0/90) interfaces, the difference in ply orientation is a maximum possible (90°); comparing to other layup angles the transverse shear stresses are expected to be the highest due to the maximum stiffness mismatch.

Transverse compressive (contact) stress (σ_{33}) is the highest on the first interface, (90/90) immediately under the indentor, and also very high on the upper interface (90/0) as shown in Fig. 6a. Interlaminar shear stress (σ_{13}) is the highest (180MPa) at the upper interface due to the effect of stiffness mismatch, Fig. 6(b). Nominal interlaminar shear strength is about 80-100MPa. However, little delamination damage was found in the upper interface in test[11]. Much published research also supports this finding that apart from a dent on the top surface, the upper interface suffers virtually no delamination damage. Mechanism of this damage suppression is due to the high compressive stress (σ_{33}) at the same location. The modelling method to account for this effect on delamination suppression is to account for the compression-induced friction stress as described in Section 2.3.

On the lower interface (0/90), the shear stress is significantly lower than that acting on the upper interface. However, the high stress level (60-80MPa in Fig. 6(b)) spreads in a larger region than that on the upper interface. Since the shear stress distribution through the thickness is a parabolic function, the shell element model calculated stress is an average stress through the thickness. The maximum shear stress is at the middle of thickness with a factor of 1.5 of the average. Comparing to the generic shear strength of 80-100MPa, it is possible to initiate delamination in the lower interface at this impact energy.

The in-plane transverse stress distribution is plotted in Fig. 7. It shows the σ_y stress in the *x-y* coordinate, which is the transverse stress component σ_{22} in the local fibre coordinate. Under the applied displacement 1·88mm, the maximum stress at the back face is about 100MPa just under the lower interface (0/90), which exceeds the resin matrix tensile strength of about 60-70MPa. Note that this analysis was without the initial stress condition caused by the elevated temperature curing process. Adding the curing process induced residual stress of about 35MPa in the resin matrix transverse to the local fibre direction (details in Ref. 29) the total σ_{22} stress is about 135MPa. Therefore, it is the σ_{22} stress component that induced matrix cracking first, which lead to delamination at the adjacent interface (0/90).

3.2 Predicted delamination size and stress distribution after damage onset

Both matrix cracking and delamination growth were modelled by the cohesive failure model under displacement-controlled QSL equivalent to impact energy 1·5J. The model takes into account the friction action on the upper interface which is under much higher compressive stress. Coefficient

https://doi.org/10.1017/S0001924000007685 Published online by Cambridge University Press

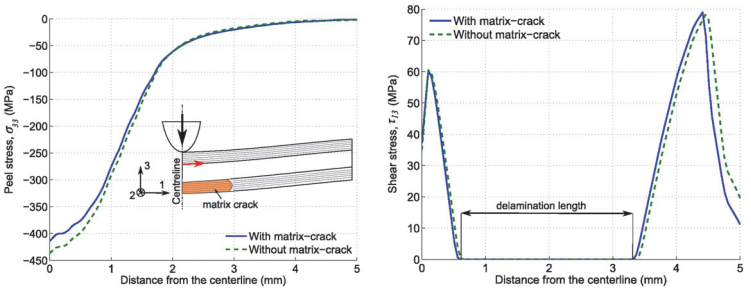


Figure 9. Computed peel (a) and shear stress (b) at the upper interface (90/0) with and without modelling matrix crack at the back face (distribution is along the lower ply fibre orientation).

of friction (μ) is selected equal to 0·9. A sensitivity study of this parameter is presented in Section 3.4. Interface elements for modelling matrix cracks were introduced along the middle line of the last stack of three 90° plies (Fig. 5). This was guided by the maximum bending deformation and resultant stress in this location. Predicted delamination area and comparison with a reference model and test measurement in[11] is shown in Fig. 8. Reasonably good agreement is achieved. Measured delamination at the upper interface was not available for this layup $(90_3/0_3)_S$, but for a specimen of stacking sequence $(0_3/90_3)_S$, which has the same geometry and same bending stiffness as the layup $(90_3/0_3)_S$, negligible delamination area was found in test on the upper interface[11,26].

Computed interlaminar peel (σ_{33}) and shear stresses (τ_{13}) at the upper interface are plotted in Fig. 9 with and without modelling matrix cracking at the bottom ply. Delamination initiation and propagation is also modelled using the aforementioned cohesive failure model. Predicted delamination length at the upper interface is about 2·5mm (Fig. 9(b)). Following observations can be made. First, the presence of a matrix crack in the specimen back face has little influence on the calculated interlaminar peel and shear stresses on the upper interface. Second, the interlaminar shear stress is the highest at the two tips of the delamination crack (Fig. 9(b)). However, the high compressive (contact) stress (Fig. 9(a)) has inhibited the propagation of delamination; consequently, despite the high shear stresses at the delamination tips, predicted damage length on the upper interface is very small as shown in Fig. 8, which agrees well with experimental observation and measurement in Ref. 26 for a similar layup $(0_3/90_6/0_3)$.

Peel stress distribution at the lower interface is plotted in Fig. 10 with and without modelling the matrix crack in the bottom ply. Without matrix crack, the peel stress is initially negative and then changes to small positive values in the lower interface along the matrix cracking direction (with only very small tensile stress directly under the indentor) (Fig. 6(a)). After matrix cracking occurs, peel stress switches to a positive value under the indentor and increases to higher values away from the indentor, which will promote the mode I delamination propagation. This observation was also reported by Chang *et al*[28]. Note that, although the trend is similar, the peel stress distribution (without modelling matrix cracking) in Fig. 10 looks different from that in Fig. 6(a). The former used shell elements, whereas the latter was modelled by solid elements. Calculated Stresses are also sensitive to mesh size.

Delamination at the lower interface is triggered by matrix cracking, which promotes the mode I delamination (since the shear stress is almost zero on the symmetry plane). Once damage onsets, it also propagates perpendicular to the matrix-crack plane, making the delamination shape wider as shown by images in Fig. 8. In order to identify the stress component that drives delamination growth in the direction transverse to matrix crack, the interlaminar shear stress on the lower

https://doi.org/10.1017/S0001924000007685 Published online by Cambridge University Press

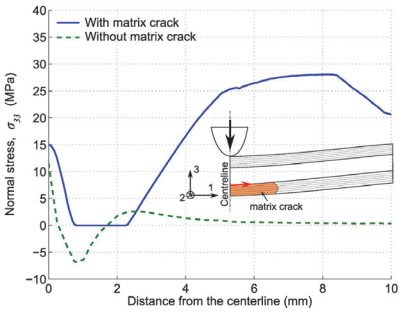


Figure 10. Peel stress distribution in the lower interface (0/90) along the matrix crack direction.

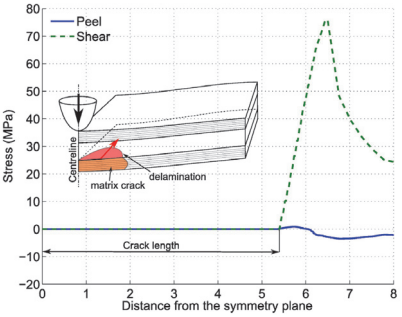


Figure 11. Shear stress (σ_{23}) distribution in lower interface along the plate span in local fibre orientation.

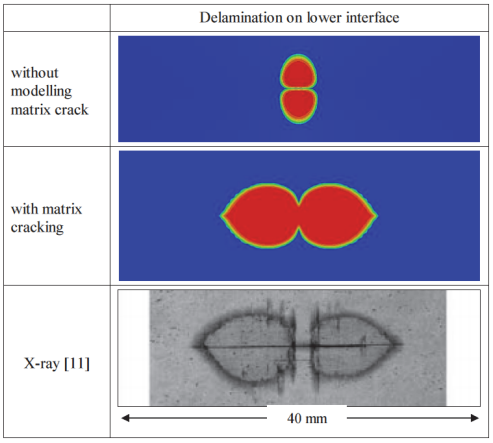


Figure 12. Predicted delamination on the lower interface with and without modelling matrix cracking (impact energy 1·5J; μ = 0·9 is used in the FE model).

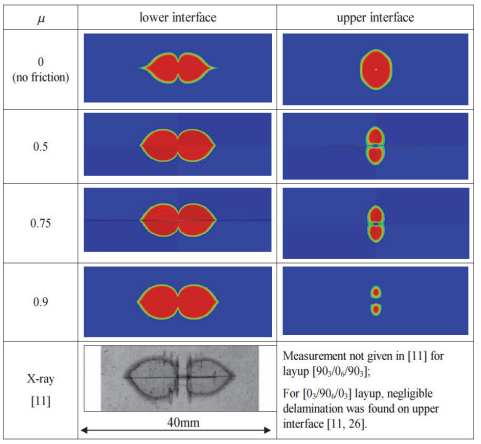


Figure 13. Comparison of predicted delamination sizes using different friction coefficients (Impact energy 1·5J) Note: the actual coefficient of friction μ_a = 0·5μ).

interface is plotted along the matrix crack direction as shown in Fig. 11. Delamination crack length at its centreline is about 5mm. Crack propagation is dominated by the mode II condition, because peel stress is almost zero and shear stress reaches peak value of 80MPa at the crack tip. Given that the average shear strength for carbon/epoxy composite is 70-100MPa, this stress level can cause delamination propagation in the transverse direction (σ_{23} is plotted in the figure).

3.3 Influence of matrix cracking on predicted delamination area

Comparison of experimental measurement with the predicted delamination shape and area (with and without allowing matrix cracking in models) is shown in Fig 12. Without modelling the matrix cracking effect, predicted delamination area is significantly smaller and also of wrong shape. The measured delamination major axis is oriented in the fibre direction of the lower ply, where the in-plane matrix crack occurred and was modelled. The matrix crack therefore triggers delamination and strongly affects the direction of the delamination crack propagation (resulting in the characteristic peanut shape). In the stacked cross-ply case, allowing a single matrix crack to initiate and propagate at the centre of the back ply has improved the model accuracy resulting in a realistic delamination shape and size.

https://doi.org/10.1017/S0001924000007685 Published online by Cambridge University Press

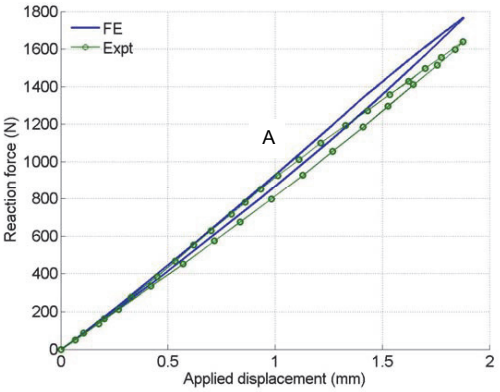


Figure 14. Force *vs* displacement: comparison of QSL model with low-velocity impact test[11].

3.4 Influence of contact-induced friction on predicted delamination size

Influence of contact force is modelled by a friction force model that inhibits delamination growth in the upper interface. The friction force is a function of the contact force and the coefficient of friction. A sensitivity analysis was conducted by using different values of the friction coefficient in the contact model. Predicted delamination areas at the upper and lower interfaces are illustrated in Fig. 13. The following observations can be made. First, much larger delamination area was predicted without considering the contact induced friction at the upper interface, demonstrating that the contact force at the interface actually inhibits the initiation and retards propagation of the delamination. Second, delamination area at the upper interface, where high contact stress acts, is very sensitive to the value of friction coefficient. However, delamination area at the bottom interface shows little sensitivity to the coefficient of friction due to much reduced contact stress on this interface. Measurement published in Ref. 30 indicates that for carbon fibre epoxy composite IM7/8552 the upper bound of friction coefficient is about 0·6 on the matrix/matrix contact face. The coefficient of friction (μ) selected for the sensitivity study is between 0·5 – 0·9. Comparing the predicted delamination size with that measured in test[11,26] for 1·5J impact energy, μ= 0·9 gives the best predicted delamination size on the upper interface. From Equations (5) and (6) and given that $K_1 = K_2$, we have $\mu_a = 0{\cdot}5\mu$ This implies that the actual coefficient of friction (μ_a) that is used for calculating the friction force using the total applied contact force (P) is 50% of the numerical friction coefficient (μ) that is inputted in the FE model for calculating the friction force based on the calculated contact force (P_c). Hence, for the best predicted delamination size in the upper interface, we have effectively used $\mu_a = 0{\cdot}45$, which is within the range of physically measured values reported in (30). Hence, it seems justified to consider using the actual coefficient of friction (μ_a) measured experimentally in Ref. 30 and to deduce the resulting coefficient of friction μ for the contact node pairs by Equation (6). The sensitivity study has shown the effectiveness of the new contact model that is relatively easy to be implemented in a commercial FE software package. It should be noted that there are other delamination inhabitant mechanisms that are not modelled in this research, e.g. the influence of the transverse compressive stresses as reported by Puck & Schürmann[31-32]. They have found that the intra- and interlaminar shear strength increases significantly under a superimposed hydrostatic stress.

https://doi.org/10.1017/S0001924000007685 Published online by Cambridge University Press

3.5 Predicted impact force *vs* displacement

Figure 14 shows predicted indentation force versus applied displacement by the QSL model. Agreement with test measurement[11] is very good up to an applied displacement of 1mm. A knee point (A) is observed in the curve measured in test and is also captured by the model. The change in slope indicates reduction in laminate stiffness due to damage. However, after point A, the model does not agree with test result well enough, implying that the change in slope may be also associated with other forms of damage, e.g. matrix cracks in locations other than the specimen centreline, which were not modelled.

It is worth mentioning that although there is significant delamination damage (Fig. 8), there is no sudden load drop before it reaches the maximum force in both test measured and model calculated force-displacement curves. This behaviour in thin laminate (about 2mm thickness) is in contrast with that observed in thicker specimens that exhibit a sudden load drop (P_{cr}) well before the peak force (e.g. 4mm thick specimen in Fig. 1). This phenomenon was also reported in the literature on impact tests on 2-2·8mm thick laminates[22,33-34], in which the critical impact force was found to be near the peak impact force. Equation (1) was deduced based on fracture mechanics assuming the presence of a delamination crack in the specimen. Since the failure of thicker specimens is dominated by shear-driven delamination, Pcr is clearly observed in the force histories (e.g. Fig. 1). For thinner laminates, damage onset is caused by matrix cracking at the back face that is induced by bending deformation of the specimen. This matrix cracking subsequently causes transverse matrix cracking and delamination at adjacent interface; hence P_{cr} is close to the peak force.

4.0 CONCLUSIONS

A numerical model has been developed for predicting low-velocity impact damage in laminated composites. It has the following new features: a) using quasi-static loading to model low-velocity impact; b) inserting cohesive elements in potential damage zones, i.e. matrix cracking and delamination; c) adding contact stiffness to cohesive elements to model the contact induced friction force. Based on the simulation of a simple cross-ply laminate ($90_3/0_6/90_3$), the following conclusions can be drawn.

- A quasi-static load model can simulate low-velocity impact induced contact force and damage.
- Matrix cracking plays an important role in initiating delamination in adjacent interface. For thin laminates the most critical matrix crack is on the back face of the specimen. Modelling matrix crack propagation by cohesive elements enables predicting delamination shape and area.
- After delamination onset, high positive peel stress develops on the lower interface along the matrix cracking direction, causing mode I delamination propagation along the lower-ply fibre orientation. This can explain the observed peanut-shape delamination with its longer axis in the fibre direction.
- Delamination also propagates in the direction transverse to matrix crack. It is mainly driven by the transverse shear stress acting on the delamination front.
- On the upper interface, mode II delamination is inhibited by the contact force induced friction stress, even though shear stress is the highest.

https://doi.org/10.1017/S0001924000007685 Published online by Cambridge University Press

ACKNOWLEDGEMENT

Liu thanks his sponsors (China AVIC and China Scholarship Council) for supporting him to study at Cranfield University, where this research was performed.

REFERENCES

1. DAVIES, G.A.O. and OLSSON, R. Impact on composite structures, *Aeronaut J*, 2004, **108**, pp 541-563.
2. ABRATE, S. *Impact on Composite Structures*, Cambridge University Press, 1998.
3. ABRATE, S. Impact on laminated composites: recent advances, *Applied Mechanics Reviews*, 1994, **47**, pp 517–44.
4. CHANG, F-K. and CHANG, K-Y. A progressive damage model for laminated composites containing stress concentrations, *J Compos Mater*, 1987, **21**, pp 834-855.
5. CHOI, H.Y. and CHANG, F.K. A model for predicting damage in graphite/epoxy laminated composites resulting from low-velocity point impact, *J Compos Mater*, 1992, **26**, pp 2134-69.
6. HOU, J.P., PETRINIC, N. and RUIZ, C. A delamination criterion for laminated composites under low-velocity impact, *Compos Sci Technol*, 2001, **61**, pp 2069-74.
7. JOHN, C.B. and PAUL, A.L. Quadratic stress criterion of initiation of delamination, *J Compos Mater*, 1988, **22**, pp 1141-55.
8. BOUVET, C., CASTANIE, B., BIZEUL, M. and BARRAU, J-J. Low velocity impact modelling in laminate composite panels with discrete interface elements, *Int J of Solids & Structures*, 2009, **46**, pp 2809-2821.
9. ZHENG, S. and SUN, C.T. A double-plate finite-element model for the impact-induced delamination problem, *Compos Sci Technol*, 1995, **53**, pp 111-8.
10. LI, C.F., HU, N., YIN, Y.J. and SEKINE, H. Low-velocity impact-induced damage of continuous fibre-reinforced composite laminates, part 1: an FEM numerical model. *Compos A*, 2002, **33**, pp 1055-62.
11. AYMERICH, F., DORE, F. and PRIOLO, P. Simulation of multiple delaminations in impacted cross-ply laminates using a finite element model based on cohesive interface elements, *Compos Sci Technol*, 2009, **69**, pp 1699-1709.
12. BORG, R., NILSSON, L. and SIMONSSON, K. Simulation of low velocity impact on fibre laminates using a cohesive zone delamination model, *Compos Sci Technol*, 2004, **64**, pp 279-88.
13. ELDER, D.J. and THOMSON, R.S., NGUYEN, M.Q. and SCOTT, M.L. Review of delamination predictive methods for low speed impact of composite laminates, *Compos Struct*, 2004, **66**, pp 677-83.
14. WISNOM, M.R. Modelling discrete failures in composites with interface elements, *Compos A*, 2010, **41**, pp 795-805.
15. SJOBLOM, P.O. and HWANG, B. Compression-after-impact: the $5,000 data point, Proc 34th Int SAMPE Symposium, Reno, Nevada, USA, 8-11 May 1989, pp 1411-21.
16. DAVIES, G.A.O. and ROBINSON, P. Predicting failure by debonding/delamination. In: Debonding/Delamination of Composites, AGARD-CP-530, Neuilly sur Seine, France, 1992, pp 5.1-5.28.
17. DAVIES, G.A.O. and ZHANG, X. Impact damage prediction in carbon composite structures, *Int J Impact Engng*, 1995, **16**, pp 149-170.
18. OLSSON, R. A review of impact experiments at FFA during 1986 to 1998. The Aeronautical Research Institute of Sweden, FFA TN 1999-08, 1999.
19. BRINDLE, A. and ZHANG, X. Predicting compression-after-impact performance of carbon fibre composites based on impact response, Proc of 17th Int Conf in Composite Materials (ICCM17), Edinburgh, UK, 27-31 July 2009.
20. Cytec Engineered Materials, Engineered Materials Technical Datasheet, www.cytec.com (accessed June 2007).
21. WIGGENRAAD, J.F.M., ZHANG, X. and DAVIES, G.A.O. Impact damage prediction and failure analysis of heavily loaded, blade-stiffened composite wing panels, *Compos Struct*, 1999, **45**, pp 81-103.
22. SJOBLOM, P.O., HARTNESS, J.T. and CORDELL, T.M. On low-velocity impact testing of composite materials, *J Compos Mater*, 1988, **22**, pp 30-52.
23. *ABAQUS User's Guide*, Version 6.10, Published by Simulia.
24. SHET, C. and CHANDRA, N. Analysis of energy balance when using cohesive zone models to simulate fracture process, *Eng Mater Technol*, 2002, **124**, pp 440-50.

https://doi.org/10.1017/S0001924000007685 Published online by Cambridge University Press

25. WILLIAMS, J.G. and HADAVINIA, H. Analytical solutions for cohesive zone models, *Mech Phys Solids*, 2002, **50**, pp 809-25.
26. AYMERICH, F., DORE, F. and PRIOLO, P. Prediction of impact-induced delamination in cross-ply composite laminates using cohesive interface elements, *Compos Sci Technol*, 2008, **68**, pp 2383-90.
27. BIANCHI, F, and ZHANG, X. A cohesive zone model for predicting delamination suppression in *z*-pinned laminates, *Compos Sci Technol*, 2011, **71**, pp 1898–1907.
28. CHANG, F.K., CHOI, H.Y. and JENG, S.T. Study on impact damage in laminated composites, *Mechanics of Materials*, 1990, **10**, pp 83-95.
29. LIU, H. Ply Clustering Effect On Composite Laminates Under Low-Velocity Impact Using FEA, MSc Thesis, Cranfield University, 2012.
30. SCHÖN, J. Coefficient of friction of composite delamination surfaces, *Wear*, 2000, **237**, pp 77-89.
31. PUCK, A. and SCHÜRMANN, H. Failure analysis of FRP laminates by means of physically based phenomenological models, *Compos Sci Technol*, 1998, **58**, pp 1045–67.
32. PUCK, A. and SCHÜRMANN, H. Failure analysis of FRP laminates by means of physically based phenomenological models, *Compos Sci Technol*, 2002, **62**, pp 1633-1662.
33. GHELLI, D. and MINAK, G. Low velocity impact and compression after impact tests on thin carbon/epoxy laminates, *Compos B*, 2011, **42**, pp 2067–79.
34. SCHOEPPNER, G.A. and ABRATE, S. Delamination threshold loads for low velocity impact on composite laminates, *Compos A*, 2000, **31**, pp 903-915.

https://doi.org/10.1017/S0001924000007685 Published online by Cambridge University Press